RSC Advances

PAPER

View Article Online
View Journal | View Issue

Cite this: *RSC Adv.*, 2018, **8**, 4239

The utilization of a three-dimensional reduced graphene oxide and montmorillonite composite aerogel as a multifunctional agent for wastewater treatment†

Yunyun Zhang,[a] Xueru Yan,[a] Yayuan Yan,[a] Dengjie Chen,[a] Langhuan Huang,[a] Jingxian Zhang,[a] Yu Ke[b] and Shaozao Tan *[a]

Received 6th December 2017
Accepted 10th January 2018

DOI: 10.1039/c7ra13103h

rsc.li/rsc-advances

Mankind has witnessed a dramatically growing challenge regarding water pollution during the past decades. Meanwhile, intensive attention has been paid to developing functional materials which can comprehensively treat wastewater which always includes bacteria, organic and inorganic contaminants. In this work, a reduced graphene oxide and montmorillonite composite (rGO–MMT) aerogel was synthesized by a one-step green method to treat multiple pollutants in wastewater. The Langmuir isotherm model and the pseudo-second-order kinetic model were well fitted to the adsorption of both dyes and heavy metal ions. The rGO–MMT aerogel exhibited 97.31% and 94.87% removal efficiencies for methylene blue (MB) and Cr(VI), respectively. In addition, the antibacterial ratios of the rGO–MMT loaded with quaternary ammonium salt reached 91.57% and 95.53% for *E. coli* and *S. aureus*, respectively. Our results demonstrated that the aerogel had a high multi-component adsorption capacity and antibacterial activity. Attractively, the rGO–MMT aerogel exhibited excellent recyclable properties thanks to its special three-dimensional structure with outstanding mechanical strength.

Introduction

There has been a major global challenge to purify sewage water since it contains organic pollutants, heavy metals and pathogens.[1] Even an extremely low concentration of 1.0 mg L^{-1} dye can contaminate drinking water and make it unavailable for human beings.[2] Moreover, most dyes are stable to photodegradation, bio-degradation and oxidizing agents.[3] Similarly, heavy metal ions like Cr(VI), Cu(II) and Pb(II) at high dosage are poisonous and carcinogenic.[4,5] At present, several physicochemical and biological methods have been applied to mediate water pollution, including flotation,[6–8] membrane separation,[9,10] adsorption,[11–13] chemical precipitation,[14,15] electrodialysis,[16] photocatalytic degradation,[17–20] and so on. Among these techniques, the adsorption process is one of the most popular methods for the removal of trace amounts of organic and inorganic pollutants from sewage due to its advantages of convenience, high removal efficiency and low cost.[21]

High-efficient adsorbent is one of the research focuses to resolve wastewater problem. Several types of materials have been investigated as adsorbents to adsorb dyes and metal ions from wastewater, including activated carbon, montmorillonite (MMT), chitosan, clay mineral, chitosan, graphene oxide (GO), reduce graphene oxide (rGO), and their composites.[22–24] Although these materials have shown excellent adsorption properties, their activity is limited in killing or inhibiting pathogens. Therefore, it has drawn intensive attention to develop adsorption material that shows antimicrobial activity for water purification. rGO, a new carbon-based material, exhibits excellent performances like high surface area, strong mechanical strength and rich surface chemistry, so it has received increasing attention.[25] Among various rGO materials, rGO aerogel is three-dimensional (3D) porous network (held together by π–π interaction and hydrogen bonding) with large specific surface area, low density and plentiful interpenetrating pore structure. Hence, it is used in the removal of oil and other organic solvents in water, which is economical and efficient.[26,27] For example, Guo *et al.* prepared chitosan–graphene oxide aerogel whose adsorption capacity of oil is 900 g g^{-1}, so it can be used to treat the industrial oil leakage or effluent in the natural water.[28] MMT is one type of layered silicate, and it has attracted extensive attention due to its abundance in various industries and low cost.[29] In view of it, it would be significant to synthesize an rGO and MMT complex to resolve wastewater problem.

[a]*Guangdong Engineering and Technology R & D Center of Graphene or Its Like Materials and Products, Department of Chemistry, Jinan University, Guangzhou 510632, P. R. China. E-mail: tsztan@jnu.edu.cn*

[b]*Department of Biomedical Engineering, Jinan University, Guangzhou 510632, P. R. China*

† Electronic supplementary information (ESI) available. See DOI: 10.1039/c7ra13103h

In this work, we synthesized a three-dimensional reduced graphene oxide and montmorillonite composite (rGO–MMT) aerogel with multi-component adsorption capacity and antibacterial activity. More importantly, the three-dimensional aerogel could sustain its initial structure after vigorous shaking when it was reused. Therefore, the three-dimensional rGO–MMT aerogel was a potential candidate as efficient adsorbent in water purification.

Experimental

Synthesis of rGO–MMT aerogel

GO originated from graphite powder was synthesized using a modified Hummers method.[30,31] The rGO–MMT aerogel was obtained by sol–gel method. Briefly, GO powder (30 mg) and ascorbic acid (30–45 mg) were added into 10 mL of ultrapure water (>18 MΩ). Meanwhile, 4 mL of MMT aqueous solution with the content ranging from 2 wt% to 6 wt% was added in order to optimize the concentration. After ultrasonic treatment for 0.5 h, the mixed solution was transferred into a 25 mL glass bottle with cover and heated at 95 °C for 6 h (for antibacterial experiment, 1 mol of dodecyl dimethyl benzyl ammonium chloride (1227) was added to the mixed solution). Then, rGO–MMT hydrogel and 1227-loaded rGO–MMT hydrogel were immersed into 6 mg mL^{-1} polyvinyl alcohol (PVA) aqueous solution for 2 days. Finally, the hydrogel was washed with ultrapure water for several times, and then fully freeze-dried at −55 °C for 12 h to acquire rGO–MMT aerogel and rGO–MMT–1227 aerogel.

Characterizations

X-ray diffraction (XRD) patterns were obtained using X-ray analyzer (MSAL-XD2) with a Cu Kα radiation source (λ = 1.5405 Å) at a voltage of 48 kV and a current of 30 mA. Characterization was performed under the 2θ range of 5.0–80.0° at a scanning rate of 2° min^{-1}. Fourier transform infrared (FT-IR) spectra were recorded using a Nicolet 6700 spectrometer. The UV-vis spectra were measured by a Hitachi 330 UV-vis spectrophotometer. Transmission electron microscopy (TEM) images and the corresponding mappings were obtained by using Philips TECNAL-10 transmission electron microscope. Scanning electron microscopy (SEM) images and energy dispersive X-ray spectroscopy (EDX) patterns were performed on a field emission-scanning electron microscope (PHILIPS XL-30 ESEM, Netherlands). The surface area and porosity of aerogel were measured by ASAP-2010 and calculated with Brunner–Emmett–Teller (BET) method. The heavy metal content of the aqueous solution was determined by inductively coupled plasma (ICP) (Optima 2000DV).

Adsorption investigation

Removal of dye. First, stock solutions (100 mg L^{-1}) of methyl orange (MO) and methylene blue (MB) were prepared by dissolving prescribed amounts of MO and MB with ultrapure water. The mixed aqueous solution of MB and MO, where the concentration of MO aqueous solution was fixed at 50 mg L^{-1} and the concentration of MB aqueous solution ranged from 5 to 50 mg L^{-1}, was prepared by diluting the stock solution. Then, the rGO–MMT aerogel was put into the conical flask containing the mixed aqueous solution, and the conical flask was kept into the shaker at 150 rpm and room temperature. 4 mL of suspension was collected at predetermined time interval for the analysis of residual dye concentration in the aqueous solution. The concentration of dye was determined with an UV-vis spectrophotometer.

Removal of heavy metal ion. The effect of initial concentration on the evaluation of the adsorption capacity was investigated by using Cr(VI) solution prepared from the standard stock solution (100 mg L^{-1}). The effect of pH value on the adsorption capacity was also investigated in the range from 2 to 11. The pH was adjusted by using 0.1 mol L^{-1} sodium hydroxide (NaOH) or hydrochloric acid (HCl) solution. Temperature was dominated in order to get the optimized adsorption. Cr(VI), Cu(II) and Pb(II) solutions were added together for the evaluation of the competitive adsorption of rGO–MMT aerogel. The concentration of heavy metal ion was determined with ICP.

Antibacterial activity. The antibacterial activity was evaluated on Gram-positive bacteria *Staphylococcus aureus* (*S. aureus*) and Gram-negative bacteria *Escherichia coli* (*E. coli*). First, the *E. coli* and *S. aureus* cells were cultured. Second, rGO–MMT, rGO–MMT-1227 and pure 1227 were added into a tube and then mixed into 10^5 cfu mL^{-1} *E. coli* or *S. aureus* with 0.85% saline. Then, all samples were immersed into bacteria at 37 °C in an orbital shaker for 24 h. Afterwards, immersed suspensions were inoculated to the medium of nutrient agar in incubator at 37 °C for 24 h. Finally, the antibacterial activity was evaluated by the reduction percentage of microorganism (R%).

$$R\% = (A - B) \div A \times 100\%$$

where A (cfu mL^{-1}) and B (cfu mL^{-1}) stood for the untreated sample and the treated sample, respectively, measured at the indicated contact time.

Results and discussion

Characterization of aerogel

According to the digital photos of rGO–MMT aerogel (Fig. 1a and b), it was obviously that the volume of rGO–MMT aerogel was larger than that of rGO aerogel. The compressive strength of rGO–MMT aerogel was examined as shown in Fig. 1c. Fig. 1d depicted a digital image of kapok with rGO–MMT aerogel was placed on the top. The insignificant deformation of kapok indicated the low density of the rGO–MMT aerogel.

XRD patterns of GO, rGO, MMT and rGO–MMT aerogel were shown in Fig. 2a. For GO, a diffraction peak at $2\theta = 10.30°$ was observed, and the calculated interlayer spacing was 0.87 nm, corresponding to the (001) plane. Meanwhile, a new broad diffraction peak at $2\theta = 24.9°$ was observed for the reduced GO, revealing the successful formation of rGO. For MMT, a well-defined diffraction peak at $2\theta = 6.12°$ appeared, which indicated the formation of a calcium montmorillonite.[32] The diffraction pattern of rGO–MMT aerogel contained the

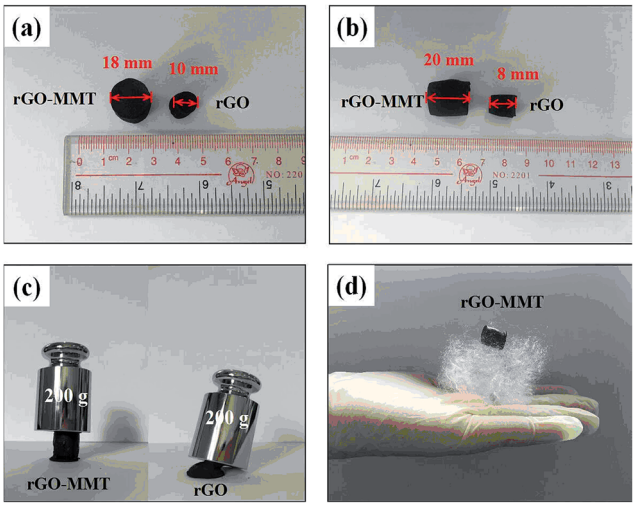

Fig. 1 The digital photos of rGO–MMT aerogel.

diffraction peaks of both rGO and MMT, indicating the successful incorporation of MMT into rGO. FT-IR spectra of GO, rGO, MMT and rGO–MMT aerogel were shown in Fig. 2b. The strong peak at 3452 cm^{-1} was attributed to the stretching vibration of the O–H. The peaks at 1731, 1621, 1384 and 1049 cm^{-1} could be assigned to the C=O, C–H–O, C=C and C–O–C, respectively. However, the O=C–O was negligible for rGO. The abundance of oxygen-containing functional group was much more on GO than that on rGO. For the FT-IR spectrum of MMT, the peaks at 3620 and 796 cm^{-1} corresponded to the stretching vibrations of the Al–OH and Si–O groups, and the strong speaks at 1089 and 1035 cm^{-1} originated from the Si–O vibration of amorphous silica and the tetrahedral sheet. Furthermore, the bands at 914, 844, 624 and 518 cm^{-1} were ascribed to deformation vibrations of Al–Al–OH, Al–Mg–OH and Si–O–Al. For rGO–MMT aerogel, all peaks belonging to rGO and MMT appeared simultaneously, and the intensity of the peak belonging to rGO became weak. These results demonstrated that rGO and MMT were combined together successfully.

The N_2 adsorption–desorption isotherms of rGO, rGO–MMT-0.02, rGO–MMT-0.04 and rGO–MMT-0.06 aerogels (Fig. S1†) exhibited type IV isotherms, according to the IUPAC classification.[33] According to the Table S1 and Fig. S2† the application of 0.04 wt% MMT was beneficial for the dispersion of rGO and the enhanced adsorption capability. Thus, rGO–MMT-0.04 was selected in subsequent experiments.

According to the SEM and TEM images (Fig. 3 and 4), there were many apparent wrinkles on the surface of rGO due to the scrolled rGO sheets. Fig. 3b, c, 4d and 3e showed that the surface of rGO–MMT aerogel was quite loose with large pore compared to rGO aerogel. The EDX (Fig. 3f) and mapping (Fig. 4d) results of rGO–MMT aerogel suggested the existence of C, O, Mg, Al, Si and Ca elements. According to the nominal existence of Mg, Al, Si and Ca elements, it could be inferred that the small particles on rGO–MMT aerogel were MMT.[32]

Adsorption experiments

Adsorption of dye. The adsorption experiment of MO was performed at room temperature without adjusting pH. rGO–MMT aerogel was added to 200 mL of MO solutions with different concentrations ranging from 5 to 50 mg L^{-1}.

Fig. 5a showed the removal of MO with different contact time. The results indicated that there was a rapid uptake within the first 20 min and then the trend became smooth. This phenomenon indicated that the surface of adsorbent was gradually blocked by dye molecules during the adsorption process, and then the surface was completely covered after certain time.[34] The adsorption curves showed that rGO–MMT rapidly adsorbed MO at the concentration of 50 mg L^{-1}, so this concentration of MO was applied in the mixed aqueous solution in subsequent experiments.

The selective adsorption of MB from mixed aqueous solution was studied, where the MO aqueous solution (50 mg L^{-1}, 200 mL) was mixed with different concentrations of MB aqueous solution (from 5 to 50 mg L^{-1}). As shown in Fig. 5b, the influence of temperature (30 °C, 40 °C and 50 °C) on the selective adsorption capacity of MB (C_0 = 40 mg L^{-1}) was investigated. A

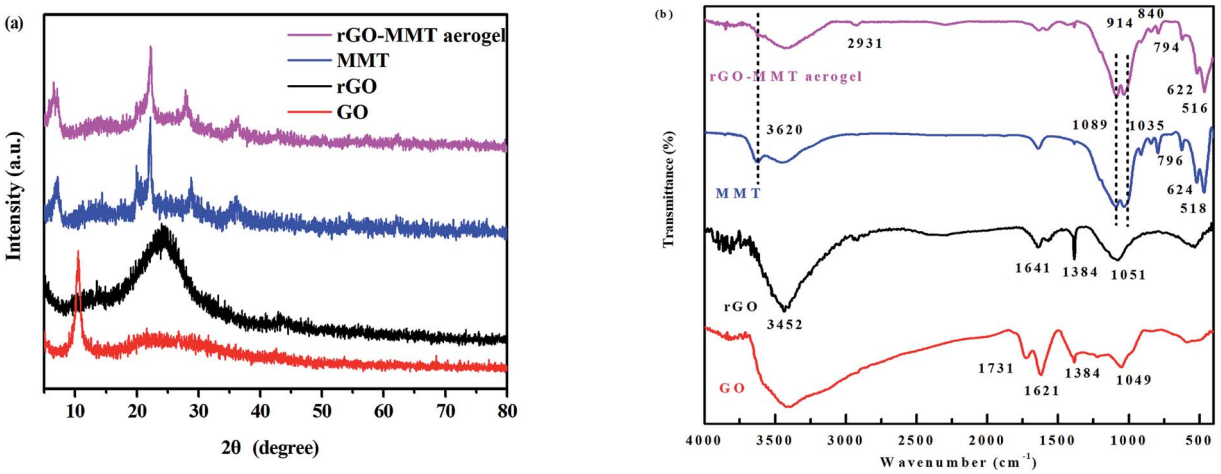

Fig. 2 XRD patterns of rGO, GO, MMT and rGO–MMT aerogel (a), FT-IR spectra of GO, rGO, MMT and rGO–MMT aerogel (b).

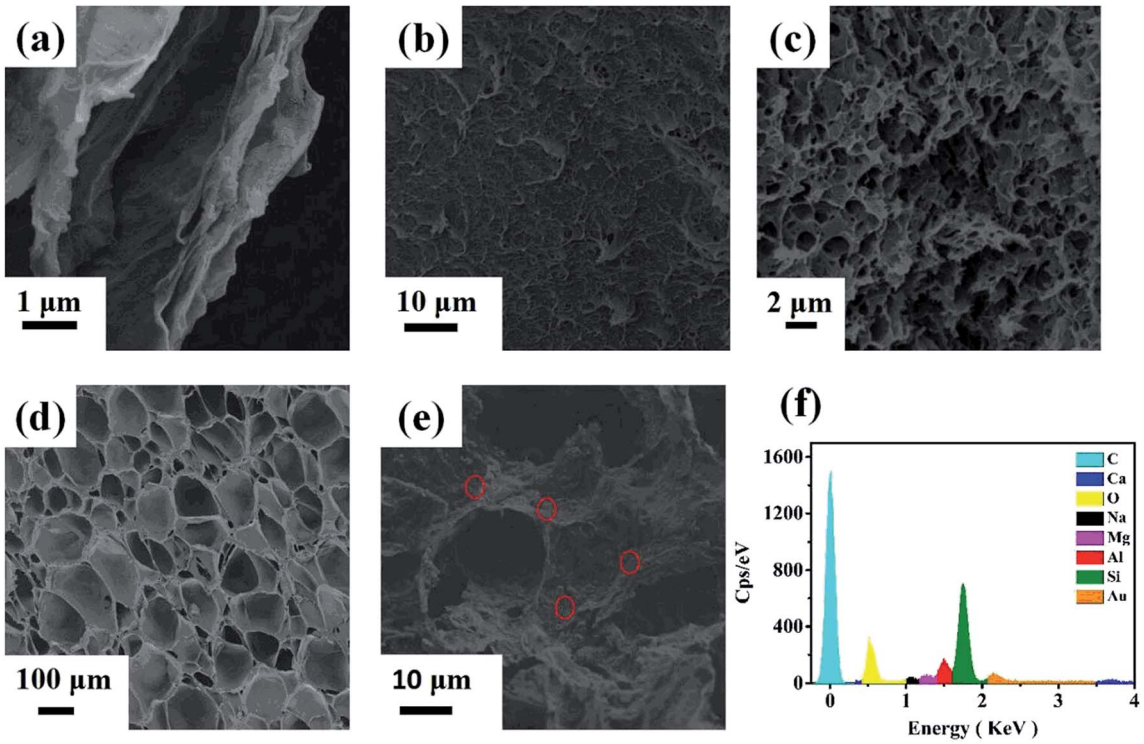

Fig. 3 SEM images of rGO (a), rGO aerogel (b and c) and rGO–MMT aerogel (d and e). EDS of rGO–MMT aerogel (f).

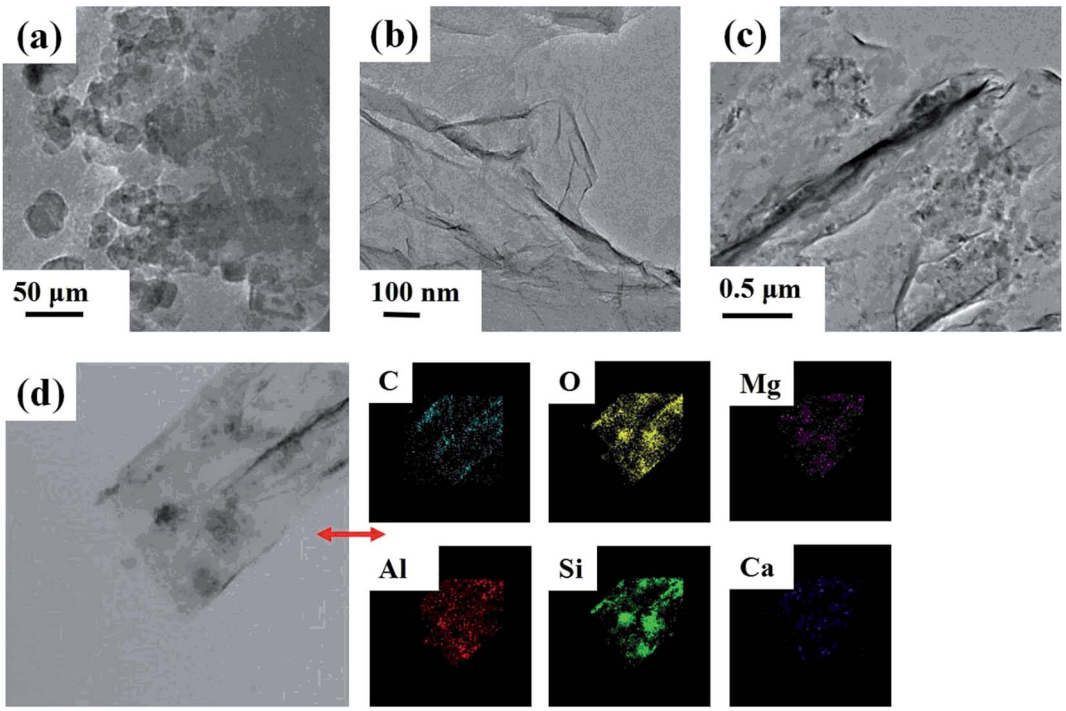

Fig. 4 TEM images of MMT (a), rGO aerogel (b) and rGO–MMT aerogel (c). Mapping of rGO–MMT aerogel (d).

high temperature promoted the diffusion rate of dye molecule, which influenced the selective adsorption of MB. However, high temperature operation would increase the cost. Thus, temperature of 40 °C was adopted for the following experiments. The pH in the solution might influence dye adsorption by changing the surface charge of the adsorbent and also the distribution of the dye in solution phase.[35] Fig. 5c showed the maximum selective adsorption capacity of MB from the mixed aqueous

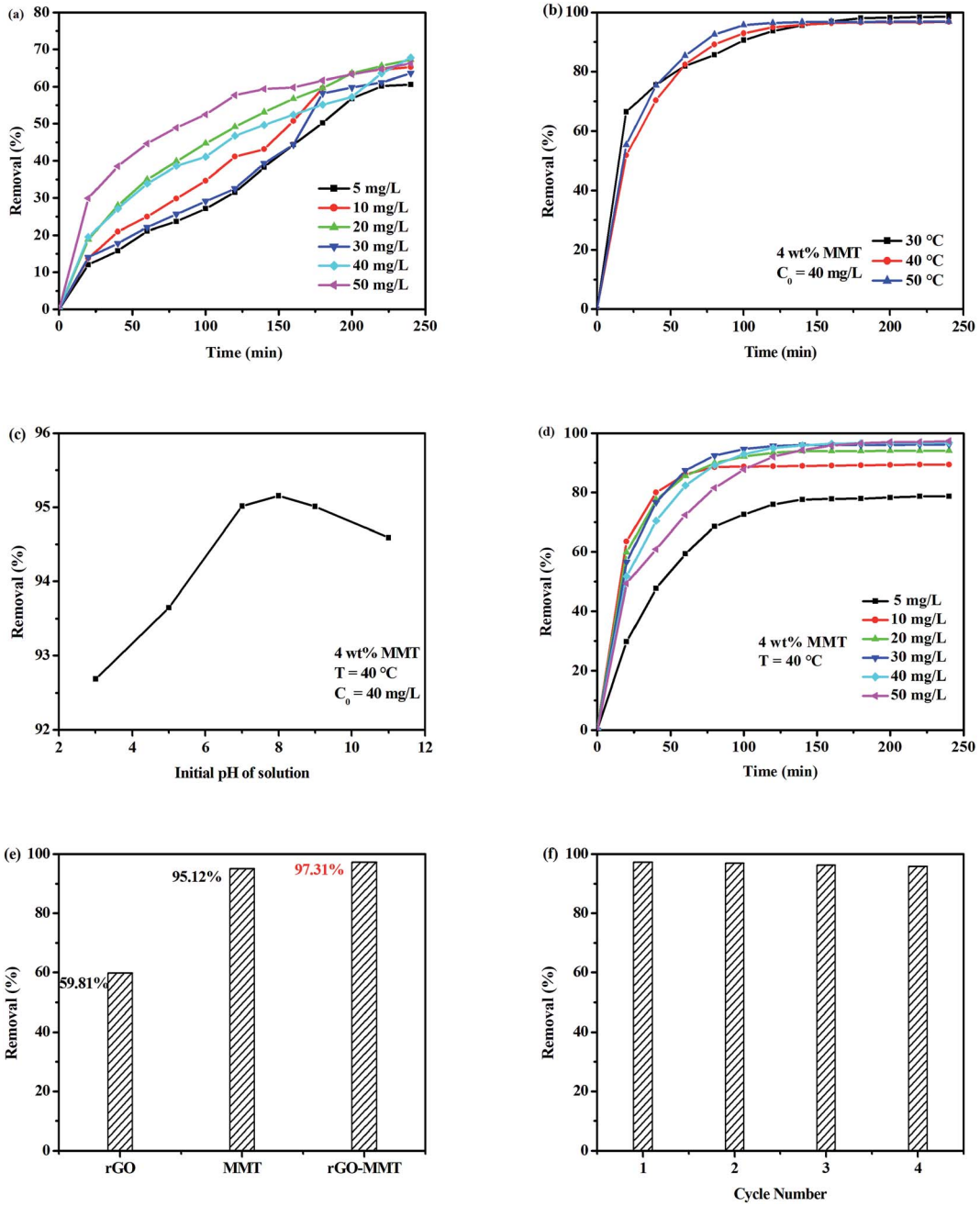

Fig. 5 Adsorption curves of MO (a), effects of temperature (b) and pH (c) on the selective adsorption of MB, effect of the concentration on the selective adsorption of MB (pH = 8 and $T = 40$ °C; the concentration of MO was 50 mg L^{-1}) (d), the selective adsorption of MB with rGO aerogel, MMT powder and rGO–MMT aerogel (e), cycle stability of rGO–MMT aerogel for the selective adsorption of MB (f).

solution by rGO–MMT aerogel at pH = 8. The selective adsorption capacity of MB from mixed aqueous solution by rGO–MMT aerogel increased with increasing pH when pH < 8, while the selective adsorption capacity of MB decreased with increasing pH from 8 to 11. Hydroxyl ions increased, and negative charges of hydroxyl ions competed with negative charges of rGO–MMT aerogel about MB. While we analyzed residual dye concentration in the aqueous solution. There were little MB combined by hydroxyl ions in aqueous solution, so the selective adsorption capacity of MB decreased. The adsorption curves showed that rGO–MMT largely adsorbed MO at the concentration of 50 mg L^{-1} (Fig. 5d). Thus, temperature of 40 °C, 4 h, pH = 8 and the concentration of 50 mg L^{-1} were selected in subsequent experiments.

Fig. 5e presented the comparison of MB selective removal rate by rGO–MMT aerogel, pristine MMT powder and rGO aerogel. rGO–MMT showed the highest removal rate of MB compared with rGO and MMT. rGO showed negligible removal rate of MB, while the removal rate of MB on MMT was 95.12%. It was difficult to recollection for suspended MMT powder in

solution. From Fig. 5f, after four adsorption/desorption cycles, it was observed that in the first cycle the selective removal rate of MB onto the rGO–MMT aerogel was 97.31% at 40 °C and pH = 8. Moreover, after four absorption/desorption cycles the removal rate still remains at 95.87%, which just reduced 1.44% compared with that of the first cycle. Remarkably, after four times cycles, the aerogels could still maintain their 3D structure. This showed that aerogel could be an environmental, high-efficient adsorbent for selective removing MB.

In this study, Langmuir (1) and Freundlich isothermal models (2) were used to understand the thermodynamics of selective adsorption of MB.[36,37]

$$\frac{C_e}{Q_e} = \frac{1}{Q_m k_L} + \frac{C_e}{Q_m} \quad (1)$$

$$\log Q_e = \log k_F + \frac{1}{n} \log C_e \quad (2)$$

where K_L (L mg^{-1}) was the Langmuir adsorption isotherm constant related to the adsorption energy; K_F (mg g^{-1}) and $1/n$ were Freundlich constants related to the capacity and intensity of adsorption; C_e (mg L^{-1}) was the equilibrium value.

Kinetics analysis was deployed for a better understanding of the selective adsorption process. The pseudo-first-order and pseudo-second-order equations were further used to model the kinetics data using a linear fitting.[36,37] The models were expressed in eqn (3) and (4):

$$\ln(Q_e - Q_t) = \ln Q_e - k_1 t \quad (3)$$

$$\frac{t}{Q_e} = \frac{1}{k_2 Q_e^2} + \frac{t}{Q_e} \quad (4)$$

where k_1 and k_2 were the pseudo-first-order and the pseudo-second-order rate constants; Q_e was the amount of MB adsorbed at equilibrium (mg g^{-1}); Q_t (mg g^{-1}) was the amount of the selective adsorption varying with time.

The fitted parameters in Langmuir and Freundlich models for selective adsorption were shown in Table 1. By comparing the R^2 values of both models, Langmuir model was better to describe the selective adsorption onto the rGO–MMT aerogel than Freundlich model, suggesting the monolayer or homogeneous adsorption for MB.[37]

The kinetics data of the adsorbent were fitted to the pseudo-first and second-order model, as shown in Fig. 6. The calculated kinetics parameters from two models were listed in Table 2. In Fig. 6a and b, the pseudo-second-order model displayed a good

Table 1 Langmuir and Freundlich isotherm parameters and correlation coefficients for the selective adsorption of MB onto rGO–MMT

	Langmuir			Freundlich		
T (K)	Q_{max} (mg g^{-1})	K_L	R^2	K_F	n	R^2
303	167.79	0.94	0.973	33.28	5.51	0.836
313	182.15	0.12	0.979	33.52	6.04	0.855
323	227.27	0.19	0.987	32.31	9.92	0.825

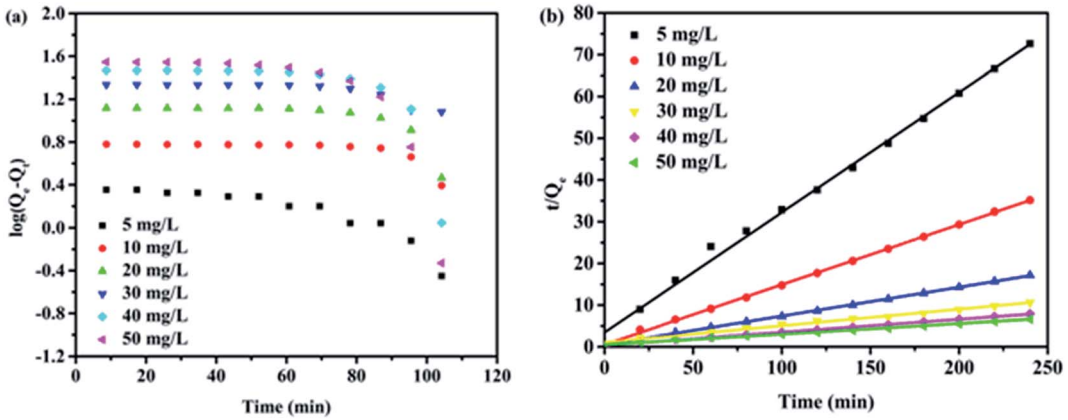

Fig. 6 Pseudo-first-order (a) and pseudo-second-order (b) equations in the modeling of adsorption kinetics.

Table 2 Kinetic parameters for the selective adsorption of MB onto the rGO–MMT aerogel in aqueous solution

Initial MB (mg L^{-1})	Pseudo-first-order			Pseudo-second-order		
	K_1	Q_e (mg g^{-1})	R^2	K_2	Q_e (mg g^{-1})	R^2
5	0.016	3.44	0.770	0.00024	3.48	0.995
10	0.0053	7.23	0.415	0.00035	6.94	0.999
20	0.0092	18.12	0.442	4.46	14.45	0.999
30	0.0053	25.95	0.606	1.47	25.19	0.984
40	0.019	57.45	0.403	2.74	32.05	0.996
50	0.029	94.01	0.506	1.36	39.22	0.992

fit with the selective adsorption of MB on rGO–MMT aerogel, while the pseudo-first-order model did not fit well, suggesting that the selective adsorption process might be based on chemisorption, involving valence force *via* sharing or exchanging electron between adsorbent and adsorbate.[38] As known, the abundant functional groups were located in rGO–MMT aerogel, such as hydroxy groups, epoxide groups and carboxylic groups. Accordingly, MB could be adsorbed *via* interaction between MB molecule and these functional groups of rGO in the rGO–MMT aerogel.

Adsorption of heavy metal ion. We had shown that the rGO–MMT aerogel had the ability to adsorb organic pollutants. In this part, the possibility of removing heavy metal ion from waste water was investigated.

Fig. 7a showed the effects of initial concentration and contact time on the removal rate. It was evident that the adsorption of heavy metal ion on the aerogel increased gradually with increasing contact time. Therefore, we selected the contact time of 4 h in this work. Totally, a low concentration of Cr(VI) was beneficial for improving removal rate. Fig. 7b showed that the adsorption capacities of Cr(VI) were 52.64%, 92.05%, 94.87%, 85.60% and 85.06% for rGO–MMT aerogel at 0 °C, 20 °C, room temperature (35 °C), 40 °C and 60 °C, respectively. The pH of the initial solution determined the charge on the surface of adsorbent and the degree of ionization and speciation of the metal ion.[39] The effect of pH on the adsorption of Cr(VI) was evaluated by changing the initial pH from 2 to 11.

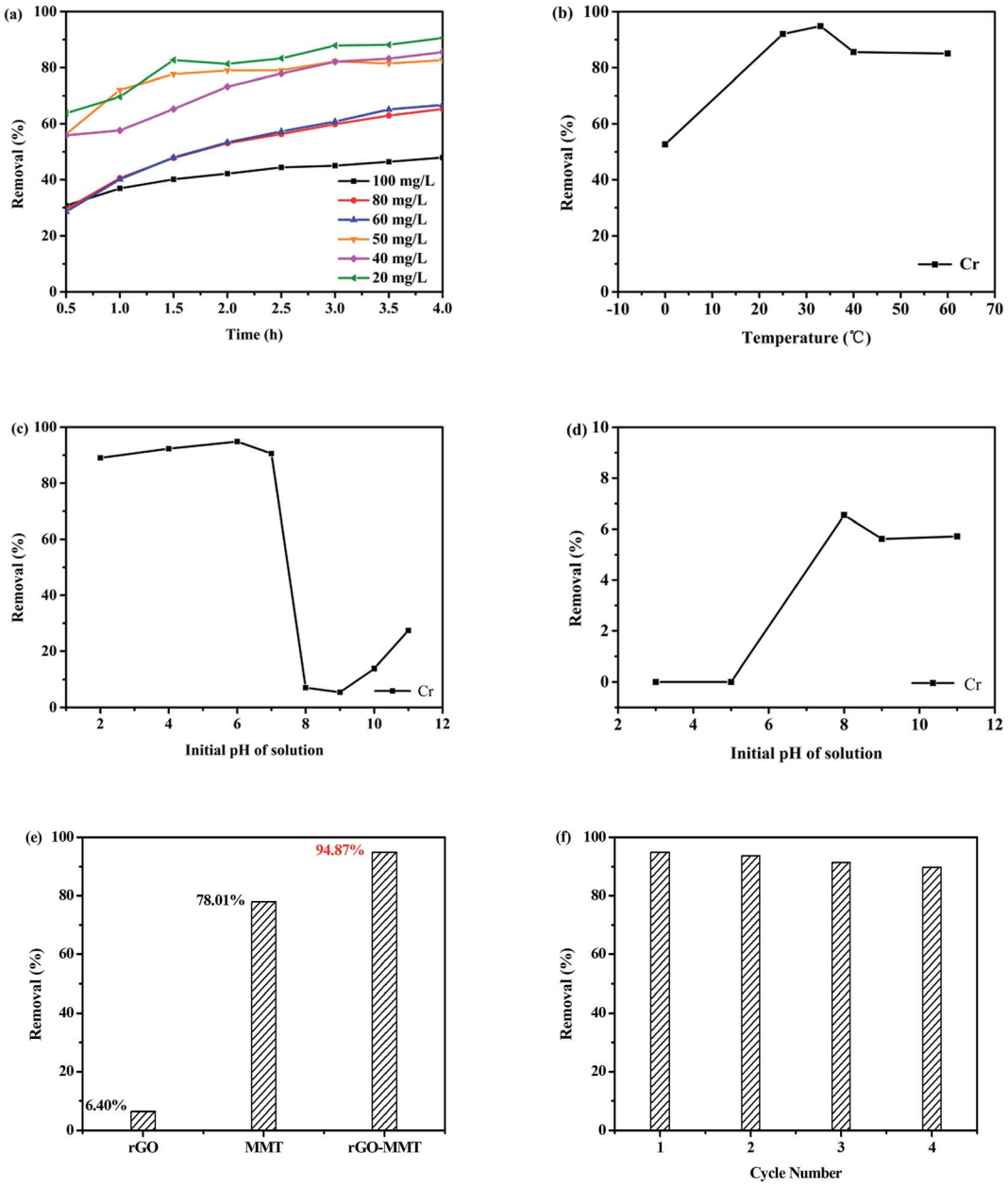

Fig. 7 Effects of initial concentration and contact time (a), temperature (b) and pH (c and d) on Cr(VI) removal with rGO–MMT, adsorption of Cr(VI) with pure rGO, MMT and rGO–MMT aerogel (e), cycle stability of rGO–MMT aerogel for the removal of Cr(VI) (f).

According to Fig. 7c and d, maximum removal rate of metal ion could be observed at pH = 6. Under the alkaline condition, the surface of the adsorbent was surrounded with OH^- that competed with CrO_4^{2-}. Meanwhile, Cr^{6+} would be reduced to Cr^{3+} to react with OH^-, and $Cr(OH)_3$ was formed. Therefore, the removal rate increased slightly when pH ranged from 8 to 11. In contrast, heavy metal ions were adsorbed due to the electrostatic adsorption at low pH.[40]

Fig. 7e presented the comparison of Cr(VI) removal rate by rGO–MMT, pristine MMT and rGO. rGO–MMT showed the highest removal rate of Cr(VI) compared with rGO and MMT. Compared with sole rGO and MMT, the effectiveness of rGO–MMT might be ascribed to a relatively large surface area, high pore volume and loose structure. We thus proposed that the synergy between rGO and MMT contributed to the enhancement of the removal rate of Cr(VI).

The adsorption of Cr(VI) was performed at pH = 6, 4 h and room temperature, and desorption with NaOH solution at pH = 13, 12 h, room temperature to evaluate the regenerate of rGO–MMT. As shown in Fig. 7f. It had no obvious decrement after four recycles, suggesting the good removal stability of the aerogel. In conclusion, our results had demonstrated that environment-friendly rGO–MMT aerogel was a robust and efficient adsorbent.

To evaluate the multiple adsorption of rGO–MMT for heavy metal ions, 10 mg L^{-1} $Cu(NO_3)_2$, 10 mg L^{-1} $Pb(NO_3)_2$ and 20 mg L^{-1} $K_2Cr_2O_7$ were mixed together in the solution. As shown in Fig. S3† it was evident that rGO–MMT could not only adsorb Cr(VI), but also adsorb Cu(II) and Pb(II).

Adsorption isotherms were important for analyzing the adsorption mechanism. The Langmuir and Freundlich models were employed to derive possible mechanism.[36,37] As shown in Table 3, it was easy to find that the fitting degree (R^2) of Langmuir model was larger than that of Freundlich model, suggesting the monolayer adsorption.[37] Besides, the Q_{max} values calculated from the Langmuir isotherm and Freundlich isotherm were 77.519 mg g^{-1} and 27.613 mg g^{-1}, respectively.

Table 3 Langmuir and Freundlich isotherm parameters and correlation coefficients for the removal of Cr(VI) with rGO–MMT

	Langmuir			Freundlich		
T (K)	Q_{max} (mg g^{-1})	K_L	R^2	K_F	n	R^2
303	77.52	0.344	0.989	27.61	3.497	0.815

Table 4 Kinetic parameters for the removal of Cr(VI) with rGO–MMT

Initial Cr (mg L^{-1})	Pseudo-first-order			Pseudo-second-order		
	K_1	Q_e (mg g^{-1})	R^2	K_2	Q_e (mg g^{-1})	R^2
20	0.0135	9.48	0.9924	0.00176	29.24	0.998
40	0.0152	38.83	0.9547	0.000490	58.48	0.992
50	0.0191	27.59	0.8349	0.00109	66.23	0.999
60	0.0157	67.20	0.9198	0.00205	75.76	0.987
80	0.0142	73.99	0.9674	0.000182	98.15	0.997
100	0.0126	36.84	0.9881	0.000122	78.74	0.998

To analyze the kinetics of Cr(VI) adsorption onto rGO–MMT aerogel, the pseudo-first-order and pseudo-second-order models were applied at different initial concentrations of Cr(VI). According to Fig. 8 and Table 4, the correlation factors of the pseudo-second order model of all initial Cr(VI) concentrations were higher than those of the pseudo-first order model. In addition, the calculated Q_e values were well in accord with the experiments. Thus, the adsorption process of Cr(VI) onto rGO–MMT aerogel followed the pseudo-second order model, suggesting the rate limiting step was the chemisorption involving the valence force.[37]

Antibacterial activity. The antibacterial activities (Fig. 9) were tested against *S. aureus* and *E. coli* bacteria, which were generally considered as standard test strains for Gram-positive and Gram-negative bacteria, respectively.[41] Antibacterial properties of rGO–MMT, rGO–MMT-1227 and pure 1227 were quantitatively evaluated by counting the antibacterial ratios of bacteria colonies before and after incubation for 24 h at 37 °C. The anti-*E. coli* ratios treated with rGO–MMT, rGO–MMT-1227 and pure 1227 reached 53.75%, 80.18%, 91.57% and 98.25%, and the counterparts were 63.39%, 91.51%, 95.53% and 99.78%. The anti-*E. coli* and anti-*S. aureus* ratios of rGO–MMT were only 53.75% and 63.39%, which obviously increased when 1227 was

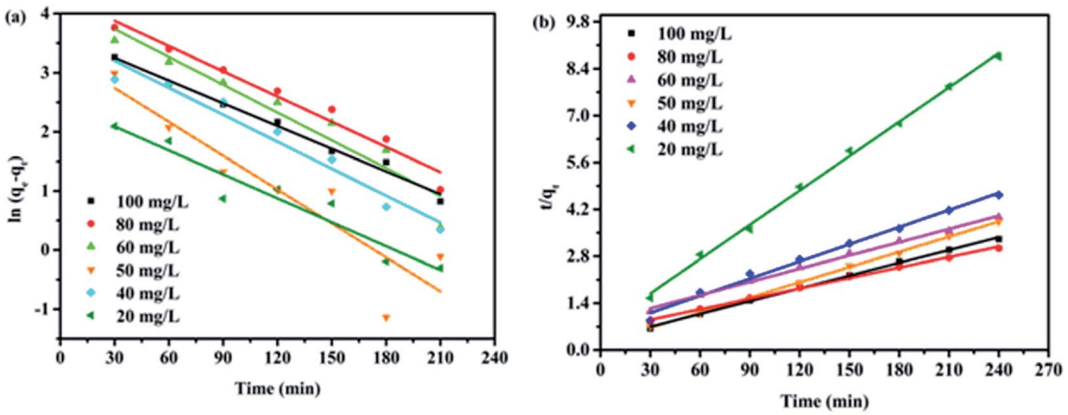

Fig. 8 Pseudo-first-order and pseudo-second-order equations in the modeling of Cr(VI) removal kinetics.

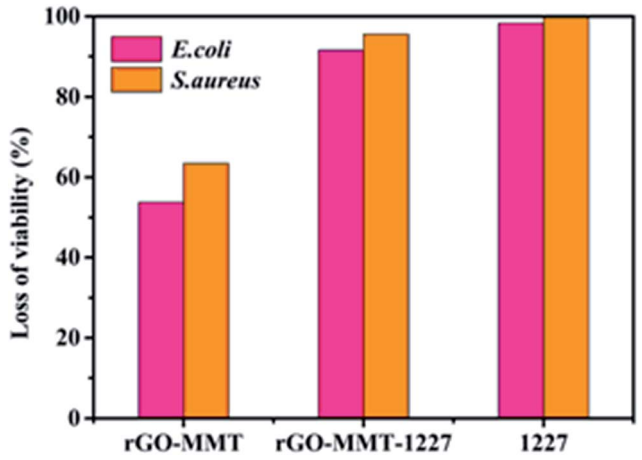

Fig. 9 Antibacterial activities of rGO–MMT, rGO–MMT-1227 and pure 1227.

added, suggesting that rGO–MMT could be applied as carrier to reduce the dosage of antibacterial agent.

Conclusions

MMT had been successfully embedded in layer of rGO, which was demonstrated by various characterizations. The prepared rGO–MMT had shown a porous structure and large specific surface area compared to sole rGO. According to adsorption studies, the Langmuir isotherm model and the pseudo-second-order kinetics model could be applied to explain the adsorption mechanisms of dyes and heavy metal ions. We had proposed that the monolayer or homogeneous adsorption was dominant, and the chemisorption involving valence force was the rate limiting step. Moreover, the maximum selective adsorption capacity of MB from the mixed aqueous solution was 227.27 mg g^{-1} and the adsorption capacity of Cr(VI) was 77.52 mg g^{-1}. In addition, the antibacterial ratios of rGO–MMT-1227 reached 91.57% and 95.53% for *E. coli* and *S. aureus*. The prepared rGO–MMT aerogel could be served as an efficient and robust material with multiple functions to handle dyes, heavy metal ions and pathogens. Therefore, the rGO–MMT aerogel was promising for water purification.

Conflicts of interest

There are no conflicts to declare.

Acknowledgements

The authors acknowledged financial support from the National Natural Science Foundation of China (21676116, 21271087 and 21476052), the Foundation of Enterprise-University-Research Institute Cooperation from Guangdong Province and the Ministry of Education of China (2015B090903072, 2015A010105019 and 2013B090600148), and the Science and Technology Innovation Platform Project of Foshan City (2015AG10020 and 2014AG100171).

References

1 X. L. Qu, P. J. J. Alvarez and Q. L. Li, *Water Res.*, 2013, **47**, 3931–3946.
2 M. T. Yagub, T. K. Sen, S. Afroze and H. M. Ang, *Adv. Colloid Interface Sci.*, 2014, **209**, 172–184.
3 L. Peng, P. F. Qin, M. Lei, Q. R. Zeng, H. J. Song, J. Yang, J. H. Shao, B. H. Liao and J. D. Gu, *J. Hazard. Mater.*, 2012, **209**, 193–198.
4 R. K. Misra, S. K. Jain and P. K. Khatri, *J. Hazard. Mater.*, 2011, **185**, 1508–1512.
5 V. C. Renge, S. V. Khedkar and S. Pandey, *Sci. Rev. Chem. Commun.*, 2012, **2**(4), 580–584.
6 M. X. Wu, J. J. Liang, J. Tang, G. Li, S. P. Shan, Z. H. Guo and L. Deng, *J. Hazard. Mater.*, 2017, **337**, 189–197.
7 S. Aoudj, A. Khelifa and N. Drouiche, *Chemosphere*, 2017, **180**, 379–387.
8 M. Kaya, *Waste Manag.*, 2016, **57**, 64–90.
9 M. C. Tomei, D. M. Angelucci, V. Stazi and A. J. Daugulis, *Sci. Total Environ.*, 2017, **599**, 1056–1063.
10 Y. J. Juang, E. Nurhayati, C. P. Huang, J. R. Pan and S. M. Huang, *Sep. Purif. Technol.*, 2013, **120**, 289–295.
11 M. R. Awual, *Chem. Eng. J.*, 2016, **303**, 539–546.
12 D. Ocinski, I. Jacukowicz-Sobala, P. Mazur, J. Raczyk and E. Kociolek-Balawejder, *Chem. Eng. J.*, 2016, **294**, 210–221.
13 Y. D. Zou, X. X. Wang, A. Khan, P. Y. Wang, Y. H. Liu, A. Alsaedi, T. Hayat and X. K. Wang, *Environ. Sci. Technol.*, 2016, **50**, 7290–7304.
14 C. E. Barrera-Diaz, V. Lugo-Lugo and B. Bilyeu, *J. Hazard. Mater.*, 2012, **223**, 1–12.
15 J. Wu, L. M. Ma, Y. L. Chen, Y. Q. Cheng, Y. Liu and X. S. Zha, *Water Res.*, 2016, **92**, 140–148.
16 A. Abou-Shady, *Chem. Eng. J.*, 2017, **323**, 1–18.
17 S. G. Kumar and K. S. R. K. Rao, *Appl. Surf. Sci.*, 2017, **391**, 124–148.
18 O. Gimeno, J. F. Garcia-Araya, F. J. Beltran, F. J. Rivas and A. Espejo, *Chem. Eng. J.*, 2016, **290**, 12–20.
19 X. F. Yang, J. L. Qin, Y. Jiang, K. M. Chen, X. H. Yan, D. Zhang, R. Li and H. Tang, *Appl. Catal., B*, 2015, **166**, 231–240.
20 M. Mehrjouei, S. Muller and D. Moller, *Chem. Eng. J.*, 2015, **263**, 209–219.
21 M. Hua, S. J. Zhang, B. C. Pan, W. M. Zhang, L. Lv and Q. X. Zhang, *J. Hazard. Mater.*, 2012, **211**, 317–331.
22 X. Guo, B. Du, Q. Wei, J. Yang, L. Hu, L. Yan and W. Xu, *J. Hazard. Mater.*, 2014, **278**, 211–220.
23 M. Karnib, A. Kabbani, H. Holail and Z. Olama, *Energy Procedia*, 2014, **50**, 113–120.
24 S. Pandey, *J. Mol. Liq.*, 2017, **241**, 1091–1113.
25 Y. Q. Guo, X. Y. Sun, Y. Liu, W. Wang, H. X. Qiu and J. P. Gao, *Carbon*, 2012, **50**, 2513–2523.
26 C. Li and G. Q. Shi, *Nanoscale*, 2012, **4**, 549–5563.
27 J. Y. Cai, W. J. Liu and Z. H. Li, *Appl. Surf. Sci.*, 2015, **358**, 146–151.
28 X. Guo, L. Qu, S. Zhu, M. Tian, X. Zhang, K. Sun and X. Tang, *Water Environ. Res.*, 2016, **88**, 768–778.

29 K. Peng, L. J. Fu, X. Y. Li, J. Ouyang and H. M. Yang, *Appl. Clay Sci.*, 2017, **138**, 100–106.
30 D. C. Marcano, D. V. Kosynkin, J. M. Berlin, A. Sinitskii, Z. Z. Sun, A. Slesarev, L. B. Alemany, W. Lu and J. M. Tour, *ACS Nano*, 2010, **4**, 4806–4814.
31 L. Z. Li, Z. Wang, P. M. Ma, H. Y. Bai, W. F. Dong and M. Q. Chen, *J. Polym. Res.*, 2015, **22**, 150.
32 M. H. Yeh and W. S. Hwang, *Mater. Trans.*, 2006, **47**, 2753–2758.
33 W. Mulewa, M. Tahir and N. A. S. Amin, *Chem. Eng. J.*, 2017, **326**, 956–969.
34 R. Boopathy, S. Karthikeyan, A. B. Mandal and G. Sekaran, *Environ. Sci. Pollut. Res.*, 2013, **20**, 533–542.
35 T. Santhi, S. Manonmani, V. S. Vasantha and Y. T. Chang, *Arabian J. Chem.*, 2016, **9**, 466–474.
36 M. A. P. Cechinel, S. M. A. G. U. de Souza and A. A. U. de Souza, *J. Cleaner Prod.*, 2014, **65**, 342–349.
37 W. Y. Huang, D. Li, Z. Q. Liu, Q. Tao, Y. Zhu, J. Yang and Y. M. Zhang, *Chem. Eng. J.*, 2014, **236**, 191–201.
38 N. Tekin, A. Safakli and D. Bingol, *Desalin. Water Treat.*, 2015, **54**, 2023–2035.
39 R. Garcia, J. Campos, J. Alfonso Cruz, M. Elena Calderon, M. Elena Raynal and G. Buitron, *TIP, Rev. Espec. Cienc. Quim.-Biol.*, 2016, **19**, 5–14.
40 T. Li, J. F. Shen, S. T. Huang, N. Li and M. X. Ye, *Appl. Clay Sci.*, 2014, **93**, 48–55.
41 A. Azam, A. S. Ahmed, M. Oves, M. S. Khan, S. S. Habib and A. Memic, *Int. J. Nanomed.*, 2017, **7**, 6003–6009.